A mass matrix formulation for cohesive surface elements

Jack Hetherington[a,*], Harm Askes[a]

[a] *University of Sheffield, Department of Civil and Structural Engineering, Mappin Street, Sheffield S1 3JD, UK*

Abstract

A well-known method for modelling crack propagation in structural finite element analysis is the use of interface elements employing the theory of cohesive surfaces. However, the use of cohesive surfaces in explicit dynamics is problematic since they have zero mass and must initially be very stiff in order to avoid the introduction of artificial compliance. These properties lead to an often drastic reduction in the critical time step of the analysis. In this paper we use the bipenalty method to derive a mass matrix for a 2D cohesive surface interface element that does not add net physical mass to the overall system. This allows for cohesive surfaces with very high initial stiffness that have no effect on the critical time step of the analysis. Not only does this lead to a more robust and stable system, it also greatly simplifies the choice of parameters since there is no need to adjust the time step, and no need to limit the initial penalty stiffness according to time step stability considerations.

Keywords: interface elements, cohesive surfaces, explicit dynamics, mass penalty, bipenalty, critical time step

1. Introduction

In finite element (FE) analysis the three most common techniques for the modelling of fracture and crack propagation in a dynamic setting are the element deletion method, the extended finite element method (XFEM), and inter-element crack methods [23]. Each of these approaches build upon standard FE formulations to include the effects of damage and crack propagation in some way. Element deletion is the simplest of the methods and the most

*Email address: cip09jeh@sheffield.ac.uk

widely used in commercial codes (e.g., ANSYS [15] and LS-DYNA [9]). It requires only an alteration of the constitutive relation of a failing element so that the stress in the element is reduced to zero for large strain, effectively removing certain elements as an analysis is carried out. However, its reliability with regards to the prediction of crack paths has been called into question [23]. Furthermore, crack paths and the details of crack growth are often highly mesh-dependent [10]. XFEM was first introduced by Belytschko and co-workers in 1999 to tackle crack propagation problems in elastostatics [3, 17]. It uses shape function enrichment in order to introduce discontinuities within finite elements, which overcomes the high mesh dependence of previously existing techniques. This makes it an attractive option for accurately and efficiently predicting crack paths which are not known a priori [5], but has yet to achieve widespread adoption in commercial software.

Inter-element crack methods are a well-established group of techniques that explicitly model cracks on the boundaries of individual finite elements. This can be achieved either by adaptive remeshing or by the addition of interface elements at element boundaries possessing a specially designed traction-displacement relationship, an approach also referred to as the cohesive zone model. The theory of cohesive surfaces (also known as cohesive zones) was first introduced in the 1960s [6, 2] but was not applied to dynamic crack propagation until the 1990s, with publications from Xu and Needleman [26], Camacho and Ortiz [4] and Repetto et al. [20] forming the basis for the present work. Each of these formulations introduces interface elements, or 'cohesive surfaces', into the FE continuum. A nonlinear traction-displacement relationship is then chosen that approximately represents the fracture characteristics of the material. Cracks are thus free to coalesce and propagate as a natural outcome of the simulation.

Using cohesive zone modelling for explicit dynamic analysis, however, leads to some unique challenges. Explicit solvers are much more efficient that implicit schemes per time step, but because they are conditionally stable the step size must be kept below the so-called critical time step, Δt_{crit}, in order to ensure stability. For the central difference method the critical time step is given by $\Delta t_{\text{crit}} = 2/\omega_{\text{max}}$, where ω_{max} is the maximum eigenfrequency of the system. The critical time step therefore depends on mesh size, as well as material properties. Elements with high stiffness or low mass decrease Δt_{crit}, leading to extra computational expense. Interface elements in a cohesive surface formulation must initially have very high stiffness so that they do not have any adverse effect on the simulation before damage

has occurred; elements that are not stiff enough lead to 'artificial compliance' in the continuum [8, 24]. In addition, they have no mass, since they have an initial volume of zero. These properties can lead to a drastic reduction in the critical time step that is required for stability.

Camacho and Ortiz [4] avoid this problem by introducing cohesive surfaces only at the onset of damage, but this requires alterations to the FE discretisation (and thus to the computer memory requirements) as cracks propagate. Ortiz and Pandolfi [18] also select a cohesive law without an initial elastic region because this would place "stringent restrictions" on the stable time step. Espinosa and Zavattieri [8] use a large initial stiffness, but it is acknowledged by the same authors that a large penalty will have a significant impact on the critical time step, and as a result, the time step calculation includes an additional limitation in that it must take into account the cohesive surfaces as well as continuum elements. Because of this, a subcycling time integration routine is built into the formulation, adding undesirable complexity to the solution algorithm. This is deemed necessary because, as noted by Song et al., the original cohesive surface formulation developed by Xu and Needleman "induces artificial compliance due to the elasticity of the intrinsic cohesive law" [24].

Interface elements by their nature introduce large eigenvalues into the FE system; since the critical time step is inversely proportional to the maximum eigenvalue this has a detrimental effect on the critical time step. The standard analysis states that this is due to the high initial stiffness of the cohesive surface elements. However, eigenvalues may be decreased not only by decreasing the stiffness of an element, but also by adding mass. Recently, an extension of the traditional penalty method—referred to here as the bipenalty method—has been proposed that includes a mass penalty matrix alongside standard stiffness penalties in the formulation [12, 1, 19, 13, 14]. In the present work, we use the bipenalty method to provide a mass matrix for a simple cohesive surface formulation. No net physical mass is added to the system; the sum of all elements in the interface mass matrix is zero. The inclusion of the mass matrix, however, does allow for control over the eigenvalues introduced by the interface elements, and therefore control over the effect that the elements have on the critical time step. By providing a mass matrix formulation alongside the traditional stiffness penalties, the introduced eigenvalues can be controlled even when very a very large initial stiffness is used, so that interface elements and, by extension, cohesive surfaces can be used in explicit dynamics without having to reduce the critical

time step.

2. Element formulation

We assume that initially we have a structural system, discretised in space by the FE method, of the form

$$\mathbf{M}\ddot{\mathbf{u}} + \mathbf{K}\mathbf{u} = \mathbf{f} \tag{1}$$

where $\mathbf{M}$ and $\mathbf{K}$ are the assembled mass and stiffness matrix for the continuum elements, $\mathbf{u}$ is the displacement vector, $\mathbf{f}$ the external force vector, and dot notation is used to indicate time derivatives; structural damping is neglected. A bipenalty formulation results in a system of equations of the form

$$\left(\mathbf{M} + \mathbf{M}^{\mathrm{P}}\right)\ddot{\mathbf{u}} + \left(\mathbf{K} + \mathbf{K}^{\mathrm{P}}\right)\mathbf{u} = \mathbf{f} \tag{2}$$

where $\mathbf{M}^{\mathrm{P}}$ and $\mathbf{K}^{\mathrm{P}}$ are mass and stiffness penalty matrices, which for a system containing cohesive surfaces are assembled from the interface element mass and stiffness matrices, which are to be derived in this section.

The critical time step for the system is given by

$$\Delta t_{\mathrm{crit}} = \frac{2}{\omega_{\max}} \tag{3}$$

where $\omega_{\max}$ is the maximum eigenfrequency of the system. Eigenvalues are related to eigenfrequencies by $\lambda_i = \omega_i^2$ and the maximum eigenvalue is $\lambda_{\max}$. The eigenvalues can be determined by solving the generalised eigenvalue problem for the system. In the case where $\mathbf{K}^{\mathrm{P}} = R\,\mathbf{M}^{\mathrm{P}}$ (with R a scalar) it has been shown that the maximum eigenvalue $\lambda_{\max}$ of the penalised system (2) will not exceed the maximum eigenvalue $\lambda_{\max}^{\mathrm{UP}}$ of the unpenalised system (1) for the case where $R \leq \lambda_{\max}^{\mathrm{UP}}$ [14, 11]. Thus, the critical time step Δt_{crit} is not decreased by the addition of the interface elements for $R \leq \lambda_{\max}^{\mathrm{UP}}$.

We will now present a standard interface element stiffness matrix formulation, followed by the corresponding mass matrix formulation, and show that under reasonable assumptions, $\mathbf{K}^{\mathrm{P}} = R\,\mathbf{M}^{\mathrm{P}}$ (and therefore that the above analysis holds for this bipenalty cohesive surface formulation).

2.1. Element stiffness matrix

The interface element formulation is based on the work of Schellekens [21, 22], who derives a 4-noded 2D line interface element with an initial

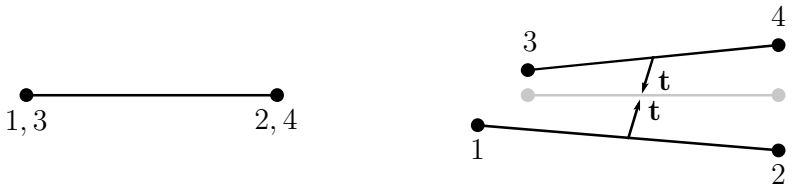

Figure 1: Line interface element in an initial (left) and deformed (right) configuration

volume of zero (see Figure 1). The stress is defined by normal and tangential tractions across the interface and the stiffness of the element is controlled by user-defined parameters that describe the constitutive behaviour.

We now consider this 4-noded line interface. Each node has two displacement degrees of freedom (DOF), giving an element nodal displacement vector

$$\mathbf{d} = [d^1_{\mathrm{n}}, d^2_{\mathrm{n}}, d^3_{\mathrm{n}}, d^4_{\mathrm{n}}, d^1_{\mathrm{t}}, d^2_{\mathrm{t}}, d^3_{\mathrm{t}}, d^4_{\mathrm{t}}]^T \tag{4}$$

where n and t denote the directions normal and tangential to the interface, respectively, and superscripts indicate the node numbers as shown in Figure 1. The relationship between nodal displacements $\mathbf{d}$ and relative displacements $\boldsymbol{\delta} = [\delta_{\mathrm{n}}, \delta_{\mathrm{t}}]^T$ is given by

$$\boldsymbol{\delta} = \mathbf{B}\mathbf{d} \tag{5}$$

where

$$\mathbf{B} = \begin{bmatrix} -\mathbf{n} & \mathbf{n} & \mathbf{0} & \mathbf{0} \\ \mathbf{0} & \mathbf{0} & -\mathbf{n} & \mathbf{n} \end{bmatrix} \tag{6}$$

and $\mathbf{n}$ are the interpolation polynomials $\mathbf{n} = [N_1, N_2]$. For arbitrarily orientated elements, the matrix $\mathbf{B}$ should be transformed to the local tangential co-ordinate system of the node set.

We now introduce a matrix $\mathbf{D}_{\mathrm{s}}$ describing the constitutive traction-displacement relation, so that

$$\mathbf{t} = \mathbf{D}_{\mathrm{s}}\boldsymbol{\delta} \tag{7}$$

where $\mathbf{t} = [t_{\mathrm{n}}, t_{\mathrm{t}}]^T$ is the traction vector for the element (units N/m^2) and $\mathbf{D}_{\mathrm{s}}$ is a constitutive matrix of the form

$$\mathbf{D}_{\mathrm{s}} = \begin{bmatrix} k_{\mathrm{n}} & 0 \\ 0 & k_{\mathrm{t}} \end{bmatrix} \tag{8}$$

The values k_{n} and k_{t} (units N/m^3) represent the 'stiffness' of the interface in the normal and tangential directions, although a more accurate description

is stiffness per unit area. It is these values that function as the stiffness penalty parameters for the interface. In the present work we assume that both parameters are equal so that $k_\mathrm{n} = k_\mathrm{t} = \alpha_\mathrm{s}$ and $\mathbf{D}_\mathrm{s} = \alpha_\mathrm{s}\mathbf{I}$. We postpone until Section 2.3 a discussion of how these constitutive relations may change over time (due to damage).

The stiffness matrix $\mathbf{K}_\mathrm{e}$ can now be obtained by minimisation of the total potential energy. The internal work done in the element is

$$U = \frac{1}{2}\int_S \boldsymbol{\delta}^T \mathbf{t} \, \mathrm{d}S \tag{9}$$

which can be rewritten using Equations (5) and (7) as

$$U = \frac{1}{2}\mathbf{d}^T \int_S \mathbf{B}^T \mathbf{D}_\mathrm{s} \mathbf{B} \, \mathrm{d}S \, \mathbf{d} \tag{10}$$

while the external work W is given by

$$W = -\mathbf{d}^T \mathbf{f} \tag{11}$$

where $\mathbf{f}$ is a vector containing the external forces on the element. After setting the variation of the total potential energy $(U + W)$ to zero we find

$$\mathbf{K}_\mathrm{e}\mathbf{d} = \mathbf{f} \tag{12}$$

where the stiffness matrix is given by

$$\mathbf{K}_\mathrm{e} = \int_S \mathbf{B}^T \mathbf{D}_\mathrm{s} \mathbf{B} \, \mathrm{d}S \tag{13}$$

Considering the numerical integration of such elements, we note that the linear shape functions can be written in one isoparametric co-ordinate ξ as

$$N_1 = \frac{1}{2}(1 - \xi) \tag{14}$$

$$N_2 = \frac{1}{2}(1 + \xi) \tag{15}$$

which means that we need integrate over only one co-ordinate. The stiffness matrix can therefore be computed using 2-point Gaussian integration via

$$\mathbf{K}_\mathrm{e} = b \int_{-1}^{1} \mathbf{B}^T \mathbf{D}_\mathrm{s} \mathbf{B} \sqrt{\left(\frac{\partial x}{\partial \xi}\right)^2 + \left(\frac{\partial y}{\partial \xi}\right)^2} \, \mathrm{d}\xi \tag{16}$$

where b is the width of the interface in the out-of-plane direction.

2.2. Element mass matrix

Thus far, we have formulated a stiffness matrix for the interface, based on the minimisation of total potential energy. In order to obtain a full bipenalty formulation, and thus obtain a suitable mass matrix, we must also consider the kinetic energy of the interface, which is related to velocity. Thus, analogous to Equation (5) we have

$$\dot{\boldsymbol{\delta}} = \mathbf{B}\dot{\mathbf{d}} \tag{17}$$

Introducing a momentum vector $\mathbf{p} = [p_\mathrm{n}, p_\mathrm{t}]^T$ we can then write a momentum-velocity relation,

$$\mathbf{p} = \mathbf{D}_\mathrm{m}\dot{\boldsymbol{\delta}} \tag{18}$$

where $\mathbf{p}$ represents momentum (per unit area) in the normal and tangential directions, and the matrix $\mathbf{D}_\mathrm{m}$ contains mass penalties in the normal and tangential directions (with units kg/m^2). It is assumed that this matrix is a scalar multiple of the constitutive matrix (25), so that $\mathbf{D}_\mathrm{s} = R\,\mathbf{D}_\mathrm{m}$, since this will simplify the implementation (and in any case, there is no apparent reason for the two penalty types to possess different normal/tangential contributions). The kinetic energy of the interface is then given by

$$T = \frac{1}{2}\int_S \dot{\boldsymbol{\delta}}^T \mathbf{p}\ \mathrm{d}S \tag{19}$$

which, after invoking (17) and (18), becomes

$$T = \frac{1}{2}\dot{\mathbf{d}}^T \int_S \mathbf{B}^T\mathbf{D}_\mathrm{m}\mathbf{B}\ \mathrm{d}S\ \dot{\mathbf{d}} \tag{20}$$

The equations of motion then follow from the minimisaton of energy

$$\mathbf{M}_\mathrm{e}\ddot{\mathbf{d}} + \mathbf{K}_\mathrm{e}\mathbf{d} = \mathbf{f} \tag{21}$$

where the mass matrix is given by

$$\mathbf{M}_\mathrm{e} = \int_S \mathbf{B}^T\mathbf{D}_\mathrm{m}\mathbf{B}\ \mathrm{d}S = \frac{1}{R}\mathbf{K}_\mathrm{e} \tag{22}$$

where

$$R = \frac{\alpha_\mathrm{s}}{\alpha_\mathrm{m}} \tag{23}$$

Since the mass matrix is therefore a scalar multiple of the stiffness matrix, it is clear that the sum of all entries is zero, and that no net physical mass is

added to the system by the interface element mass matrices. Furthermore, the stability analysis given in Reference [14] for an arbitrary set of multipoint constraints remains valid, which implies that any additional eigenvalues introduced by the addition of the interfaces will tend to the penalty ratio R for large penalty parameters. Therefore, to ensure time step stability, the ratio R should be chosen such that

$$R \leq \frac{4}{\Delta t^2} \tag{24}$$

where Δt is the chosen time step for the analysis (i.e., a time step suitable for analysis of the *unpenalised* system, without interfaces). The magnitude of the entries in $\mathbf{D}_\mathrm{s}$ and $\mathbf{D}_\mathrm{m}$ can be selected by the analyst, and may be related to the stress history in the element, as explored in Section 2.3.

It is important to note that this formulation results in a *non-diagonal mass matrix*. Since explicit methods are most efficient when a lumped, diagonal mass matrix can be used, this will inevitably have an effect on the computational efficiency of the solution algorithm. However, the system mass matrix remains diagonal except for those DOF which are penalised, and therefore the effects on solution time are usually limited. For an alternative implementation of this methodology that avoids the inversion of (part of) the mass matrix, see the recent work of Lombardo and Askes [16].

2.3. Constitutive relations and damage law

The constitutive law for the cohesive surfaces relates traction in the interface to the displacement jump across the surface. As summarised by Xu and Needleman, "the behaviour that needs to be captured is that, as the cohesive surface separates, the magnitude of the traction at first increases, reaches a maximum and then approaches zero with increasing seperation" [26, p. 1400]. However, this kind of cohesive law is problematic when used in explicit dynamics, since "the initial elastic slope ... may place stringent restrictions on the stable time step for explicit integration" [18]. In other words, the initial penalty stiffness in the interface causes a significant decrease in the critical time step of the analysis. This effect may be mitigated by decreasing the initial stiffness of the interfaces, but this leads to an increase in artificial compliance (a general decrease in the stiffness of the continuum that leads to unrealistic elastic deformation), especially when cohesive surfaces are embedded throughout the finite element mesh [25, 24]. Since the inclusion of an interface mass matrix means that such considerations are no longer relevant,

in the present formulation there is no such restriction on the initial stiffness of the interfaces.

We begin by describing the traction-displacement relationship to be employed, first by rewriting the constitutive matrix for the cohesive surface stiffness matrix as

$$\mathbf{D}_{\mathrm{s}} = \gamma_{\mathrm{s}}\mathbf{I} \tag{25}$$

where γ_{s} acts as the penalty parameter (interface stiffness), but is now dependent on a set of damage parameters. It is initially set to $\gamma_{\mathrm{s}} = \alpha_{\mathrm{s}}$, but may decrease over time as damage occurs and the interface cohesion begins to lessen.

The value of γ_{s} is determined by two scalar quantities, namely the effective opening displacement δ and the effective traction t. Inspired by the fracture criteria given by Camacho and Ortiz [4], we have for the effective opening displacement

$$\delta = \begin{cases} \sqrt{\delta_{\mathrm{n}}^2 + \beta^2\delta_{\mathrm{t}}^2} & \text{if } \delta_{\mathrm{n}} \geq 0 \\ \delta_{\mathrm{n}} & \text{if } \delta_{\mathrm{n}} < 0 \end{cases} \tag{26}$$

This value gives a measure of displacement across the interface. The parameter β dictates to what degree tangential displacements are taken into account when assessing damage in the interface. We assume that no damage occurs in compression, and hence tangential displacements are not considered when assessing relative displacement for $\delta_{\mathrm{n}} < 0$.

The effective traction depends on the current state of the interface and where it lies with regards to the cohesive law shown in Figure 2. For undamaged interfaces, the traction-displacement relation is linear-elastic. By defining the history parameter $\delta_{\max}$ as the maximum effective opening displacement reached during an analysis, we can say that the interface is undamaged if $\delta_{\max} \leq \delta_0$, where δ_0 is the effective displacement value corresponding to the onset of damage. Therefore, during this initial phase,

$$t = \alpha_{\mathrm{s}}\delta \qquad \text{if } \delta_{\max} \leq \delta_0 \tag{27}$$

where α_{s} is the initial elastic stiffness of the interface. If the effective traction should exceed the maximum value of t_c the interface enters a damaged state and the constitutive relation changes to reflect linear softening in the material, so that

$$t = t_{\mathrm{c}}\left(1 - \frac{\delta - \delta_0}{\delta_{\mathrm{c}} - \delta_0}\right) \qquad \text{if } \delta > \delta_0, \delta = \delta_{\max} \tag{28}$$

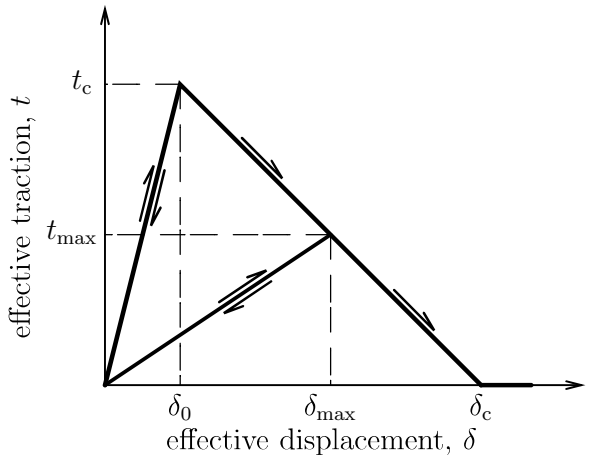

Figure 2: Cohesive law for tensile tractions, showing the loading path and a potential unloading path

If the effective displacement reaches the critical value δ_c during loading then the interface is broken irreversibly, creating a free surface, and

$$t = 0 \qquad \text{if } \delta_{max} > \delta_c \tag{29}$$

If the effective opening rate becomes negative ($\dot{\delta} < 0$) at any time *after* damage has occured then the interface is said to be unloading. In this state the constitutive behaviour is once again linear-elastic, but with a reduced stiffness. Then,

$$t = \frac{t_{max}}{\delta_{max}}\delta \qquad \text{if } \delta < \delta_{max} \tag{30}$$

where t_{max} is the effective traction corresponding to the effective displacement δ_{max}. Together, these relations describe all four of the possible states for an interface: undamaged (linear-elastic), undergoing damage (softening), unloading (linear-elastic, reduced stiffness) and broken (zero traction/free surface).

The effective penalty parameter γ_s of (25) is given by

$$\gamma_s = \begin{cases} \alpha_s & \text{if } \delta_{max} \leq \delta_0 \\ t_{max}/\delta_{max} & \text{if } \delta_{max} > \delta_0 \end{cases} \tag{31}$$

We assume that the gap across the interface does not close again after breaking. To model such problems, the definition could be extended so that the

interface has stiffness in compression ($\delta < 0$) even after the maximum displacement has been reached ($\delta_{\max} \geq \delta_c$).

At each time step, the effective relative displacement δ is computed for each interface so that any changes in the state of the interface may be detected. For affected elements the damage model is implemented by computing the associated effective tractions and then updating the constitutive matrix for those elements via Equation (25).

Finally, we introduce the cohesive fracture energy G_{c}, a fundamental parameter of the cohesive zone model regarded as a material constant, which represents the work of separation per unit area of cohesive surface. It is given by the area under the traction-displacement curve, which, for the formulation described above, gives

$$G_{\mathrm{c}} = \int_0^{\delta_{\mathrm{c}}} t \, \mathrm{d}\delta = \frac{t_{\mathrm{c}}\delta_{\mathrm{c}}}{2} \tag{32}$$

This relationships allows the traction-displacement curve to be fully described by t_c (representing the yield strength of the material), and the fracture energy G_{c}, both of which can be obtained by experimental testing of a specimen.

With the inclusion of a damage law, we must also consider how the constitutive matrix $\mathbf{D}_{\mathrm{m}}$ may change as damage occurs; i.e., identify the damage parameters which determine γ_{m} in the nonlinear constitutive matrix

$$\mathbf{D}_{\mathrm{m}} = \gamma_{\mathrm{m}}\mathbf{I} \tag{33}$$

One option is to form a new damage law specifically for the mass matrix of the element as opposed to the traditional traction-displacement used to govern the stiffness of the interface. However, this would effectively constitute a new set of velocity constraints, whereas our goal is to enforce the nonlinear displacement constraints (in the form of cohesive surfaces) which have already been derived. Consequently, we adopt the same cohesive law for both mass and stiffness matrices, which, with the reintroduction of the penalty ratio R gives $\gamma_{\mathrm{m}} = \gamma_{\mathrm{s}}/R$. The penalty ratio may be used to control the relative influence of the stiffness and mass penalty matrices. Note by adopting this method, the assumption that $\mathbf{D}_{\mathrm{s}} = R\,\mathbf{D}_{\mathrm{m}}$ (and therefore $\mathbf{K}_{\mathrm{e}} = R\,\mathbf{M}_{\mathrm{e}}$) is valid throughout the analysis.

3. Example: elastic wave propagation

In order to test the interface element formulation, we consider a rectangular region of elastic material modelled using the finite element method. A regular grid of square elements is used to mesh the domain. Two-dimensional interface elements are then inserted between the FE continuum elements in the *right* half of the mesh to observe what effect this has on wave propagation through the medium, as shown in Figure 3. At this point, the interfaces are non-breaking and do not suffer damage, and the interface constitutive matrices are given simply by $\mathbf{D}_\mathrm{s} = \alpha_\mathrm{s}\mathbf{I}$ and $\mathbf{D}_\mathrm{m} = \alpha_\mathrm{m}\mathbf{I}$ regardless of interface tractions. (This corresponds to a cohesive surface formulation where the maximum traction t_c is never exceeded.)

In the following work we define a dimensionless penalty factor that gives a measure of penalty parameter magnitude. The parameters α_s and α_m control the accuracy of constraint imposition, but are only effective if they are several orders of magnitude larger than the existing entries in the system matrices $\mathbf{K}$ and $\mathbf{M}$. We therefore define

$$p_\mathrm{s} = \frac{\alpha_\mathrm{s}}{\max\limits_{i \in P}(K_{ii})} \tag{34}$$

$$p_\mathrm{m} = \frac{\alpha_\mathrm{m}}{\max\limits_{i \in P}(M_{ii})} \tag{35}$$

where P is the set of all DOF numbers associated with the constraint. Then, the stiffness and mass penalty factors p_s and p_m give a measure of the magnitude (and therefore effectiveness) of the penalty parameters α_s and α_m, respectively.

Stress wave propagation through the rectangular system is shown qualitatively in Figure 4, for a stiffness penalised system. The material has arbitrary properties Young's modulus $E = 1$ Pa, mass density $\rho = 1$ kg/m^3, Poisson's ratio $\nu = 0$, and plane stress is assumed. The point load $F = 10^{-3}$ N is applied from the beginning of the analysis until time $t = 0.1$ s. The element side length is $h = 0.02$ m for all elements (giving a total of 5000 elements).

In order to quantify errors, a reference solution (shown in Figure 4a) is first produced by omitting interface elements entirely. By introducing interface elements with low stiffness penalty parameters, as in Figure 4b, we can easily observe the effects of the added interfaces. Note that the analysis concludes before any wave reflections occur at the boundaries of the region, and hence wave propagation on the left-hand side of the material

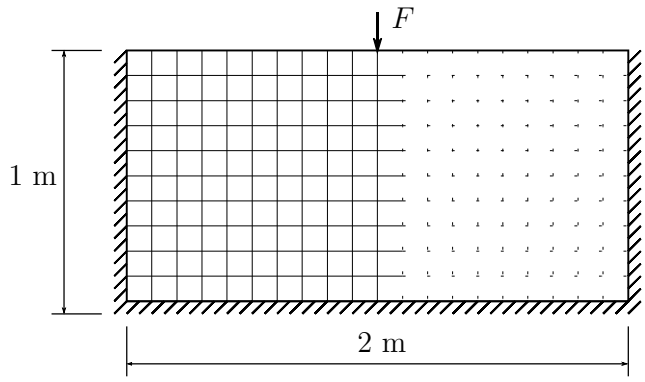

Figure 3: Diagram of rectangular elastic region showing fixed supports (indicated by hashed edges) and interface elements (dotted lines), for an element size of $h = 0.1$ m.

appear quite unaffected by the interfaces. In the interface process window, however, stress wave propagation is slowed considerably by the additional elastic strain manifesting between the continuum elements, a phenomenon known as artificial compliance. This is clearly evident in the stress error field, shown in Figure 4c.

Figure 4 demonstrates the need for well-enforced interface constraints. If no damage has occurred, a continuum that includes cohesive surfaces and the interface-free continuum should ideally behave identically, with zero displacement across an interface. Using penalty methods, this is only possible in the limit as penalty parameters tend to infinity, but cohesive surfaces can be practically transparent if the initial penalty is large enough. Of course, with stiffness-type penalties this introduces concerns with regards to time step stability.

In order to assess the performance of the stiffness, mass and bipenalty methods, we now turn our attention to the error norm of the stress profiles for a number of analysis types. Figure 5 shows the L_2 norm of the error in stress profile, $\|\mathbf{e}_\sigma\|$, between two analyses with and without penalty-based interface elements, for a range of penalty factors. Note that the quantity represented by the x-axis (penalty factor, p) represents the penalty factor that has been used as input in each case. For the stiffness penalty analyses this is the stiffness penalty factor p_s, and for the mass and bipenalty analysis it is the mass penalty factor p_m, since for the bipenalty method, the stiffness

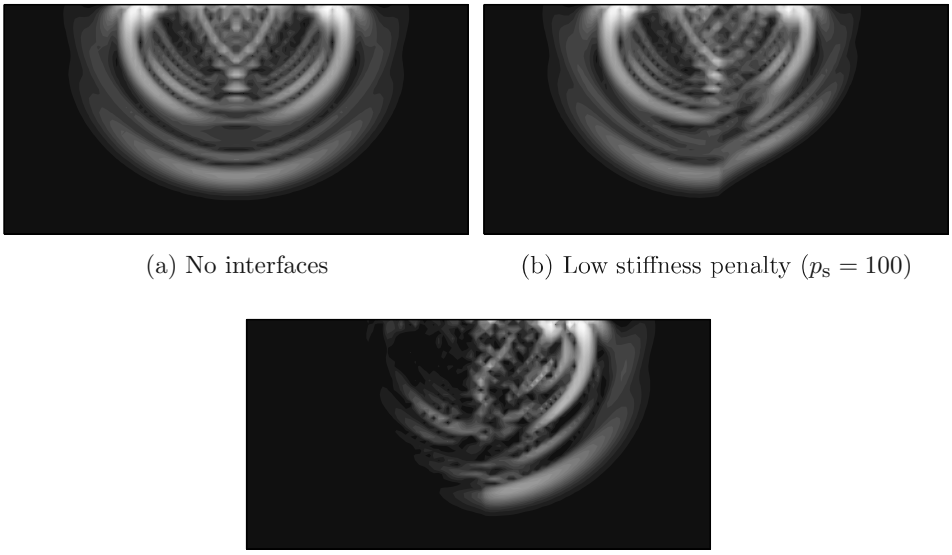

(a) No interfaces

(b) Low stiffness penalty ($p_\mathrm{s} = 100$)

(c) Absolute error field

Figure 4: Von Mises stress profiles at time $t = 0.8$ s, including error field.

parameters are calculated based on a suitable penalty ratio R.

Figure 6 shows the time steps used for the analysis on a logarithmic scale. For mass and bipenalty methods, suitable time steps are estimated using the maximum eigenvalue of all individual elements, whereas for the stiffness penalty method the maximum eigenvalue of the full constrained system must be used. This data shows that achieving high accuracy using stiffness-type penalties quickly becomes very expensive as penalty parameters are increased; indeed, for stiffness penalty factors $p_\mathrm{s} > 10^8$ the tests became prohibitively expensive.

4. Example: crack propagation in PMMA plate

For validation of the formulation in a dynamic setting, we turn our attention to an experiment carried out by Combescure et al. [5], who investigate crack propagation through a polymethyl methacrylate (PMMA) plate under impact loading. The experiment uses a Hopkinson bar to apply load to the left-hand side of the PMMA specimen shown in Figure 7, which features a

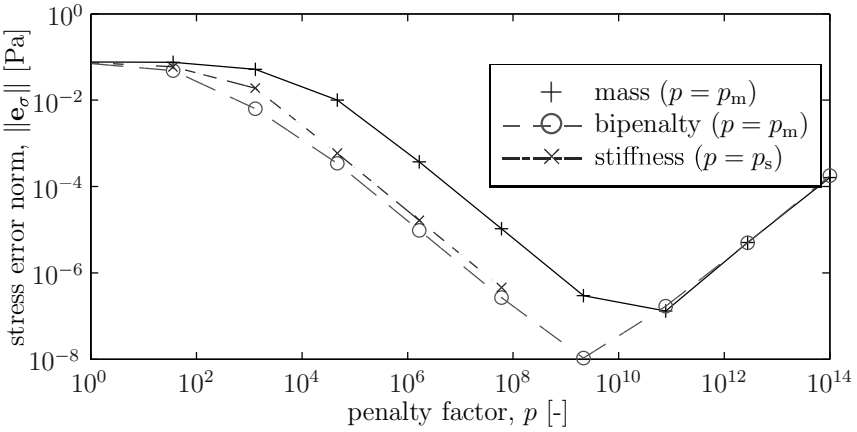

Figure 5: Stress error norm at time $t = 0.8$ s for the stiffness, mass and bipenalty methods.

pre-existing crack emanating from a central hole. The specimen suffers fracture damage during the first 500 µs after impact, and the crack tip position is measured during this time to obtain a detailed crack propagation history.

In this section we simulate the experiment numerically using bipenalty cohesive surfaces. Only the PMMA plate is considered, since the initial contact with the Hopkinson bar on the left-hand side of the specimen can be modelled with prescribed velocities, while contact at the other end is handled with absorbing boundary conditions. Given material properties for the plate include Young's modulus $E = 4.25$ GPa, mass density $\rho = 1180$ kg/m^3, Poisson's ratio $\nu = 0.42$ and fracture toughness $K_\mathrm{IC} = 1.47$ MPa$\sqrt{\mathrm{m}}$.

For the cohesive bipenalty formulation we require the damage parameters t_c and G_C (from which we can calculate δ_c). The cohesive fracture energy can be calculated from the fracture toughness via $G_\mathrm{C} = K_\mathrm{IC}^2/E$. The yield stress t_c is not given, and so initially a range of values are tested, from 10–100 kPa.

The final crack path for $t_\mathrm{c} = 15$ KPa is shown in Figure 8. Although the total length of the path is not captured by the simulation, the initial portion of the crack is reproduced very well. Note that since the crack is required to move along element boundaries it cannot generally move in a perfectly straight line, which adds extra length to the simulated crack path. This in turn adds to the amount of energy required to open the crack, which may help to explain why the numerical path is somewhat shorter than the experimental result.

The growth of the crack over time is compared to experimental obser-

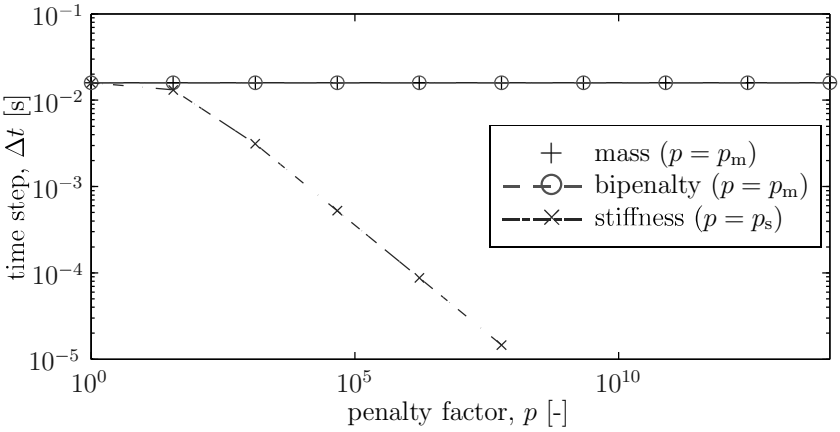

Figure 6: Time step used in each analysis (approximately $0.9\Delta t_{\mathrm{crit}}$).

vations in Figure 9. The experimental results show the crack beginning to form at around 200 µs, stopping briefly when it reaches $x \approx 90$ mm, before continuing to its end point. While in the numerical tests crack initiation is about 25 µs early, and crack speed propagation is generally higher than in experiments, the stop-start behaviour of the crack propagation is captured to some extent for $t_{\mathrm{c}} = 12$–18 kPa.

The mostly likely reason for disparities in the numerical tests is the accuracy of the bilinear cohesive law. By refining the traction-displacement relationship it may be possible to obtain more accurate results, although this would likely require access to further experimental test data for the material in question. An alternative cohesive model designed for the modelling of PMMA is given by Elices et al. [7]

However, in general the bipenalty cohesive surfaces are well-suited to this problem type, where high loading rates mean that the the explicit central difference method is an obvious choice for the solution scheme. Since stiffness-only elements lead to artificial compliance, an artificially lowered time step, or else unexpected time step instabilities, their use is problematic. On the other hand, the bipenalty method allows for time steps close to the critical time step of the unconstrained problem, while allowing for a very high initial stiffness.

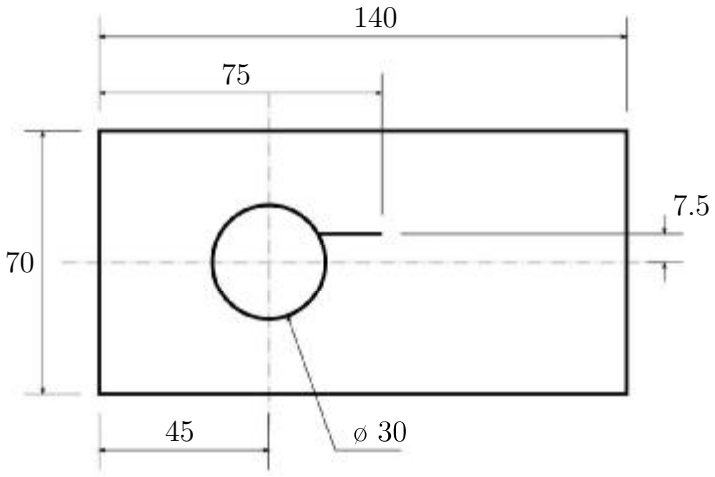

Figure 7: Geometry of the PMMA specimen (dimensions in mm).

5. Conclusion

The most significant advantage of the central difference method over implicit time integration routines is that the computations carried out at each time step are very efficient. The major disadvantage is that for stability, the size of the time step must be relatively small. Traditional penalty methods, such as those used in the formulation of cohesive surfaces, have little effect on the actual computation, but can drastically reduce the critical time step. Alternatively, the bipenalty method has no effect on the critical time step, but it increases the cost of each time step computation by requiring that the mass matrix of the system be non-diagonal.

We can therefore say that the bipenalty method is an appropriate choice only in certain situations. If high accuracy is required (high penalty stiffness, low compliance) and the number of bipenalised degrees of freedom is small relative to size of the problem, then the extra computational effort required to solve a small linear system may be offset by the fact that less time steps are needed. Furthermore, the bipenalty method may provide a more robust solution by ensuring time step stability in all circumstances, giving the analyst more freedom to select suitable parameters; but, if cohesive surfaces must be introduced throughout the whole continuum, a very large linear system of equations would need to be solved at each time step.

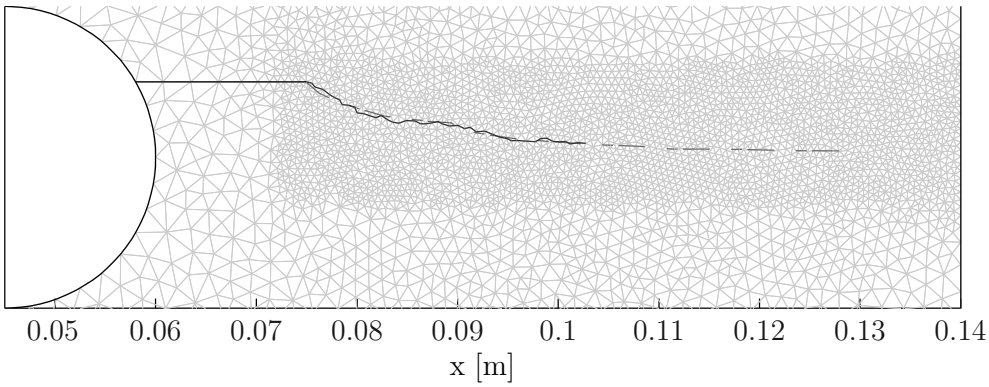

Figure 8: Experimental (red, dashed) and numerical (blue, solid) results for final crack path ($t_c = 15$ KPa).

In summary, the bipenalty method is a simple way to control the eigenvalues introduced when adding cohesive surfaces to an FE simulation. With the introduction of a single extra parameter, the penalty ratio R, the analyst can ensure that the critical time step of an explicit analysis is not affected by the interfaces. But while the bipenalty method could theoretically be employed in any explicit dynamic problem involving cohesive surfaces, whether or not the additional computational cost is justified depends entirely on the problem under consideration; specifically, the number of constraints relative to the size of the total system should be as small as possible.

[1] H. Askes, M. Caramés-Saddler, and A. Rodríguez-Ferran. Bipenalty method for time domain computational dynamics. *Proceedings of the Royal Society A: Mathematical, Physical and Engineering Sciences*, 466(2117):1389–1408, 2009.

[2] G. I. Barenblatt. The mathematical theory of equilibrium cracks in brittle fracture. *Advances in Applied Mechanics*, 7:55–129, 1962.

[3] T. Belytschko and T. Black. Elastic crack growth in finite elements with minimal remeshing. *International Journal for Numerical Methods in Engineering*, 45:601–620, 1999.

[4] G. Camacho and M. Ortiz. Computational modelling of impact damage in brittle materials. *International Journal of Solids and Structures*, 33(20-22):2899–2938, 1996.

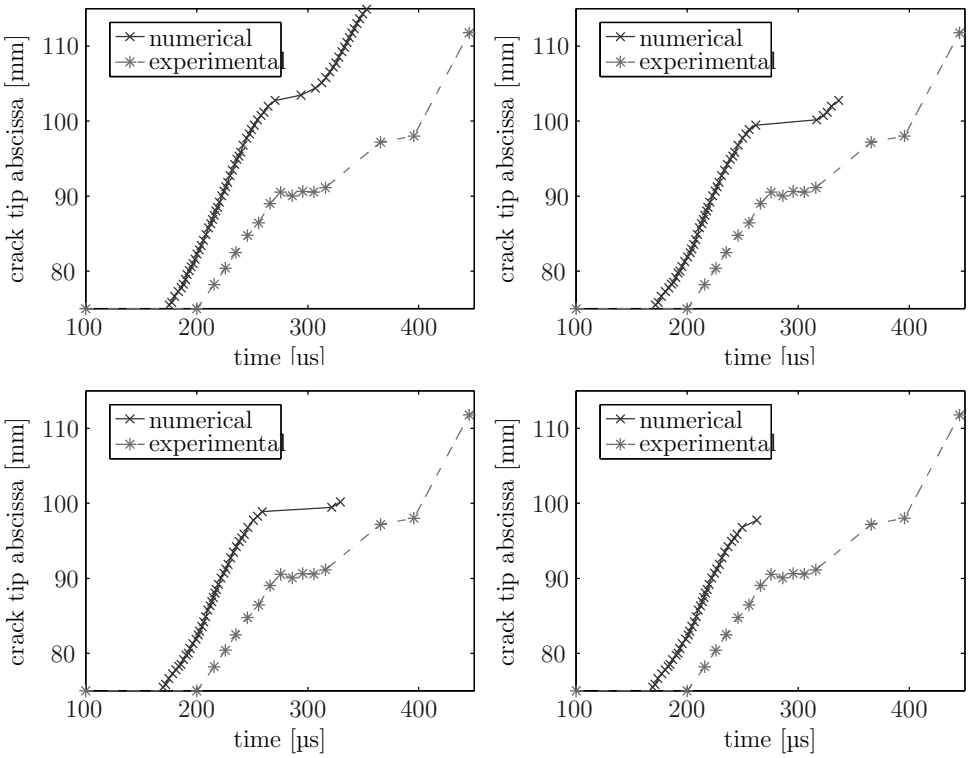

Figure 9: Position of crack tip (x-dir) over time: t_c = 12 KPa (top left), 15 KPa (top right), 18 KPa (bottom left), 21 KPa (bottom right)

[5] A. Combescure, A. Gravouil, D. Grégoire, and J. Réthoré. X-FEM a good candidate for energy conservation in simulation of brittle dynamic crack propagation. *Computer Methods in Applied Mechanics and Engineering*, 197(5):309–318, 2008.

[6] D. Dugdale. Yielding of steel sheets containing slits. *Journal of the Mechanics and Physics of Solids*, 8(2):100–104, 1960.

[7] M. Elices, G. Guinea, J. Gómez, and J. Planas. The cohesive zone model: advantages, limitations and challenges. *Engineering Fracture Mechanics*, 69(2):137–163, 2002.

[8] H. D. Espinosa and P. D. Zavattieri. A grain level model for the study of failure initiation and evolution in polycrystalline brittle materials.

Part I: Theory and numerical implementation. *Mechanics of Materials*, 35(3-6):333–364, 2003.

[9] J. O. Hallquist. *LS-DYNA Theory Manual*. Number March. Livermore Software Technology Corporation, Livermore, California, 2006.

[10] R. Hambli. Comparison between Lemaitre and Gurson damage models in crack growth simulation during blanking process. *International Journal of Mechanical Sciences*, 43(12):2769–2790, 2001.

[11] J. Hetherington. *The bipenalty method for explicit structural dynamics*. PhD thesis, University of Sheffield, 2013.

[12] J. Hetherington and H. Askes. Penalty methods for time domain computational dynamics based on positive and negative inertia. *Computers & Structures*, 87(23-24):1474–1482, 2009.

[13] J. Hetherington, A. Rodríguez-Ferran, and H. Askes. A new bipenalty formulation for ensuring time step stability in time domain computational dynamics. *International Journal for Numerical Methods in Engineering*, 90(3):269–286, 2012.

[14] J. Hetherington, A. Rodríguez-Ferran, and H. Askes. The bipenalty method for arbitrary multipoint constraints. *International Journal for Numerical Methods in Engineering*, 2012.

[15] P. Kohnke, editor. *ANSYS, Inc. Theory Reference: ANSYS release 9.0*. ANSYS, Inc., Canonsburg, 2004.

[16] M. Lombardo and H. Askes. Lumped mass finite element implementation of continuum theories with micro-inertia. *International Journal for Numerical Methods in Engineering*, 96(7):448–466, 2013.

[17] N. Moes, J. Dolbow, and T. Belytschko. A finite element method for crack growth without remeshing. *International Journal for Numerical Methods in Engineering*, 46(1):131–150, 1999.

[18] M. Ortiz and A. Pandolfi. Finite-deformation irreversible cohesive elements for three-dimensional crack-propagation analysis. *International Journal for Numerical Methods in Engineering*, 44(9):1267–1282, 1999.

[19] E. A. Paraskevopoulos, C. G. Panagiotopoulos, and G. D. Manolis. Imposition of time-dependent boundary conditions in FEM formulations for elastodynamics: critical assessment of penalty-type methods. *Computational Mechanics*, 45(2-3):157–166, 2010.

[20] E. A. Repetto, R. Radovitzky, and M. Ortiz. Finite element simulation of dynamic fracture and fragmentation of glass rods. *Computer Methods in Applied Mechanics and Engineering*, 183(1-2):3–14, 2000.

[21] J. C. J. Schellekens. *Computational strategies for composite structures*. PhD thesis, Delft University of Technology, 1992.

[22] J. C. J. Schellekens and R. De Borst. On the numerical integration of interface elements. *International Journal for Numerical Methods in Engineering*, 36(1):43–66, 1993.

[23] J.-H. Song, H. Wang, and T. Belytschko. A comparative study on finite element methods for dynamic fracture. *Computational Mechanics*, 42(2):239–250, 2007.

[24] S. H. Song, G. H. Paulino, and W. G. Buttlar. A bilinear cohesive zone model tailored for fracture of asphalt concrete considering viscoelastic bulk material. *Engineering Fracture Mechanics*, 73(18):2829–2848, 2006.

[25] M. Tijssens. *On the cohesive surface methodology for fracture of brittle heterogeneous solids*. PhD thesis, Delft University of Technology, 2000.

[26] X.-P. Xu and A. Needleman. Numerical simulations of fast crack growth in brittle solids. *Journal of the Mechanics and Physics of Solids*, 42(9):1397–1434, 1994.